Foam drainage modeling of vertical foam column and validation with experimental results

Hosseini-Nasab, S. M.; Rezaee, M.; Zitha, P. L. J.

DOI
10.1016/j.ptlrs.2024.05.001

Publication date
2024

Document Version
Final published version

Published in
Petroleum Research

Petroleum Research 9 (2024) 586–598

Contents lists available at ScienceDirect

Petroleum Research

journal homepage: http://www.keaipublishing.com/en/journals/petroleum-research/

Full Length Article

Foam drainage modeling of vertical foam column and validation with experimental results

S.M. Hosseini-Nasab [a, *], M. Rezaee [b], P.L.J. Zitha [c]

[a] School of Chemical, Petroleum and Gas Engineering, Iran University of Science and Technology, Tehran, Iran
[b] Department of Petroleum Engineering, Amirkabir University of Technology, Tehran, Iran
[c] Department of Geoscience & Engineering, Petroleum Engineering Group, Delft University of Technology, Netherlands

ARTICLE INFO

Article history:
Received 15 June 2023
Received in revised form
15 April 2024
Accepted 19 May 2024
Available online 21 May 2024

Keywords:
Foam
EOR
Drainage
Stability
Foam modelling
Foam viscosity

ABSTRACT

The understanding of the mechanisms behind foam generation and the structure of foam itself form the basis of foam-related experiments for its application in Enhanced Oil Recovery and overcoming gas injection limitations. Novel insights in this paper towards the theory of foam generation can help explain experimental results and lead to improved formulas of the applied substances and concentrations. This study aims to investigate the mechanisms behind foam generation and the structure of foam by specific laboratory experiments and theoretical analyses. The liquid drainage through interconnected Plateau borders was found to be the most critical foam decay mechanism for this particular research. The justification of the foam drainage equation was demonstrated by comparing the numerical solution with the outcome of a few bulk experiments. The discrepancies were described according to the limitations of both the theory and the experimental settings. Foam modelling gives more profound knowledge in more detail of the different stages in foam drainage than experimental data can deliver, which is because of the lack of continuous measurement of foam conductivity for the foam bulk test. Therefore, a comprehension of foam modelling investigation and comparison is required to gain a deeper understanding of foam behaviour.

1. Introduction

Foam is a two-phase system with a structure of gas cells surrounded by a continuous liquid phase in which a surfactant is dissolved (Abdelaal et al., 2020; Ardakani et al., 2020; Skauge et al., 2020; Issakhov et al., 2022). To create foam, an amount of energy is needed equal to the product of the area created and the surface tension of the liquid (Ahmed et al., 2019; Burrows et al., 2020). The foamability of the liquid is measured as the quantity of foam generated during the gas sparged through a liquid (Xu et al., 2017; Yusuf et al., 2022).

Additives to the bulk solution can modify the foam's properties, like the solution's viscosity, aiming to improve the foam's stability. The stabilizing additive aims to slow down the mechanisms that lead to the eventual decay of the foam (Roozbahani et al., 2024). Additives can stabilize the foam by decreasing the diffusion of gas, increasing the thickness of the electrical double layer, increasing the bulk viscosity of the liquid, slowing down the drainage and increasing the elasticity of the foam film (Hosseini-Nasab et al., 2015; Rezaee et al., 2022). Hydrophobic chemicals form an adsorbed layer at the interface of the gas and liquid in the film, increasing the resistance to rupture and forming a diffusion barrier. Chemicals that are hydrophilic (and consist of high molecular weight) are adsorbed in the liquid in the films, which will increase the bulk liquid viscosity and therefore slow down gravity drainage (Razavi, 2020; Hosseini-Nasab et al., 2022).

In order to research the suitability of certain fluids, solutions or other materials for oil recovery, field tests can be performed when the likelihood of success has been established by examination on a smaller scale. One of the methods of choice is core flooding, where a core sample from the subsurface can be used to measure (the change of) rock properties like permeability or be a subject of flooding by liquids and/or gases. Core flooding is relatively time-consuming, and therefore, it is helpful to perform other types of experiments to have a quicker screening of the desired subject of

* Corresponding author.
E-mail addresses: hosseininasab@iust.ac.ir (S.M. Hosseini-Nasab), mohammad.rezaee@adelaide.edu.au (M. Rezaee), P.L.J.Zitha@tudelft.nl (P.L.J. Zitha).

https://doi.org/10.1016/j.ptlrs.2024.05.001

research, which can lead to more accurate core flooding experiments.

The foaming properties of solutions can be examined in foam bulk experiments, where a foam column is created from a gas injection under controlled conditions through a liquid solution. These experiments take up less time per experiment than core flood experiments and can also be done more rapidly, while core flooding experiments need extensive cleaning time to prepare the setup for the next experiment. The behaviour of foam in porous media can be understood by examining its bulk properties, which reveal significant correlations. Foam density is a key factor, as higher density enhances stability and resistance to collapse in porous media. Foam viscosity also plays a role, with higher viscosity resulting in slower flow rates and potentially better stability. Foam stability, including resistance to coalescence and drainage, affects its behaviour in porous media, as more stable foams maintain their structure and flowability for more extended periods. The wetting properties of foam, such as its contact angle with porous media, impact its ability to displace fluids and improve sweep efficiency. Lastly, foam rheology, including elasticity and yield stress, influences its flow behaviour in porous media, potentially improving resistance to flow blockage and channeling (Yang et al., 2019; Abdelaal et al., 2020). It is essential to realize that these screening types of experiments are related to the core flood experiments but do not have a total overlap due to different experimental conditions. For example, in core flooding, the system is often pressurized to mimic subsurface conditions, leading to the different behaviour of gases compared to bulk experiments at atmospheric pressure. The foam bulk experiments form the basis for comparing non-Newtonian and Newtonian viscofying agents in foam EOR. It will show insight into the foam properties and foam behaviour in time for injected fluids containing Glycerol and polymer to see if Glycerol can be a worthy substitute for specific oil recovery projects where the use of polymer is not feasible (Emami et al., 2022).

When using polymers to stabilize foam in Enhanced Oil Recovery (EOR) processes, challenges can arise at high polymer concentrations, affecting foam capacity. Factors contributing to this behaviour include polymer adsorption, which creates a thick polymer layer around bubbles, hindering foam formation and stability (Davarpanah and Mirshekari, 2020). Viscosity increase at high concentrations impedes liquid flow and foam stability. While polymers can act as coalescence inhibitors at lower concentrations, excessive polymer layers can promote coalescence and destabilize foam at high concentrations (Hanamertani and Ahemd, 2021). Polymer-polymer interactions and shear sensitivity further impact foam stability and capacity. To overcome these challenges, careful optimization of polymer concentration and consideration of polymer characteristics are necessary. Experimentation and studying rheological properties can help determine the optimal concentration range for achieving stable foam with high capacity in EOR processes (Akbari et al., 2019; Bai et al., 2022).

Previous work in bulk foam experiments has provided tremendous information on the foaming properties of several surfactants and fluids. In previous research on surfactant screening, Alpha Olefin Sulfonate (AOS) C14–C16 showed a high foam stability in both the absence and presence of oil. When different additives are used, the creation and distribution of foam are governed by mechanisms such as surface tension reduction, stabilization of foam films, and modification of bubble size and stability. Surface tension reduction allows for easier spreading of the liquid and the formation of smaller bubbles. Stabilization of foam films prevents their rupture and collapse. Additives can also influence bubble size and stability, either inhibiting coalescence for increased stability or promoting coalescence for larger bubbles. The behaviour of additive-stabilized foams can vary depending on factors like temperature, pH, additive concentration, and the nature of the liquid. These conditions can affect foam stability and properties, emphasizing the importance of considering specific conditions when assessing the consistency of additive-stabilized foams (Hernando et al., 2016; Ahmed et al., 2019; Imuetinyan et al., 2022). Additives play a crucial role in modifying foam's physical and chemical properties to maintain its structure and prevent collapse or degradation. Several mechanisms contribute to foam stabilization, including surfactant action, viscosity modification, coalescence inhibition, and rheology modification. Surfactants reduce surface tension and form a protective layer around bubbles to prevent coalescence and drainage. Viscosity modification resists drainage and maintains foam structure. Coalescence inhibitors prevent bubble merging. Rheology modification enhances stability by providing resistance to deformation and collapse. The choice of additives and their concentrations depend on the specific application and desired foam properties, and understanding their interactions is vital for optimal foam stabilization (Yusuf et al., 2022).

Foam destruction can occur through various mechanisms when oil is present in enhanced oil recovery (EOR) applications. Some of the mechanisms behind foam destruction in the presence of oil include Coalescence: Oil droplets can coalesce with the foam lamellae, leading to the rupture and collapse of the foam structure. Drainage: Oil can displace the liquid phase in the foam column, causing drainage and thinning of the foam films. This can result in reduced foam stability and collapse. Emulsification: Oil can emulsify within the foam structure, forming oil-in-water emulsions. This can disrupt the foam stability and lead to foam destruction. Bridging: Oil droplets can bridge between foam lamellae, causing the collapse of the foam structure. These mechanisms can vary depending on factors such as the properties of the oil, the surfactant used, and the specific conditions of the EOR application. It is essential to consider these mechanisms when designing and optimizing foam-based EOR processes (Hosseini-Nasab and Simjoo, 2018; Goodarzi and Zendehboudi, 2019; Zoeir et al., 2020).

2. Theoretical backgrounds

The amount of liquid present in the foam changes throughout the foam column. As liquid drains out of the foam, the foam at the top of the column becomes drier (Hosseini-Nasab and Zitha, 2017; Wang et al., 2021). The lamellae contain very little liquid and are thin, making the foam cells take on a polyhedral shape. The structure of foam changes when it contains more than 1% liquid is present (Zhang et al., 2015; Zhao et al., 2022). The liquid is distributed in the foam column between the lamellae and Plateau borders. The increased amount of liquid in the foam is located in the Plateau borders. As the liquid fraction in the foam increases (for example, due to the continuous addition of liquid on top of the foam column), the shape of the Plateau borders changes (Imuetinyan et al., 2022). The edges of the gas bubbles become rounder when liquid is added until no more liquid can be stored in the foam, as exhibited in Fig. 1.

Foam is the limit of a wet foam, and the bubbles are of a spherical shape. When less liquid is present in the foam, the shape of the bubbles deforms to a polyhedral shape, and thin films of the bulk liquid are present at the locations where the deformed bubbles are in contact (Hosseini-Nasab et al., 2016; Bouquet et al., 2019).

From Fig. 2, it can be observed that wet foam exhibits the closest packing. It also shows the foam cells' shape change for changing liquid content. As foam becomes drier and the films become thinner, the viscosity of the foam increases (Yu and Saraji, 2021; Dong et al., 2016).

According to the Fig. 3, the molecules inside the bulk liquid are

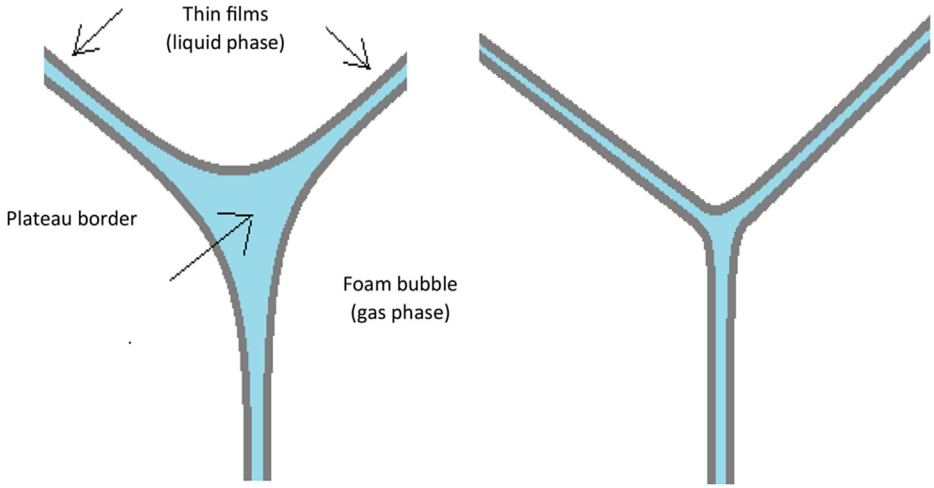

Fig. 1. The large liquid volume in the Plateau border wet foam (left) and the small liquid volume in the Plateau in a dry foam (right).

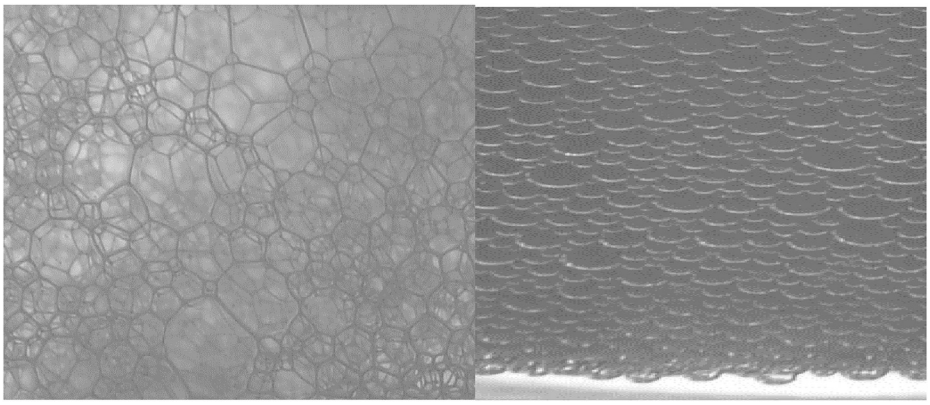

Fig. 2. Left: As the foam begins to dry, the liquid content decreases, and the bubbles start to deform against each other, transitioning into a polyhedral structure. Right: Wet foam bubbles stays spherical shape. In a wet foam, the bubbles maintain a nearly spherical shape because they are closely packed with a visible layer of liquid between them, allowing them to only loosely contact each other.

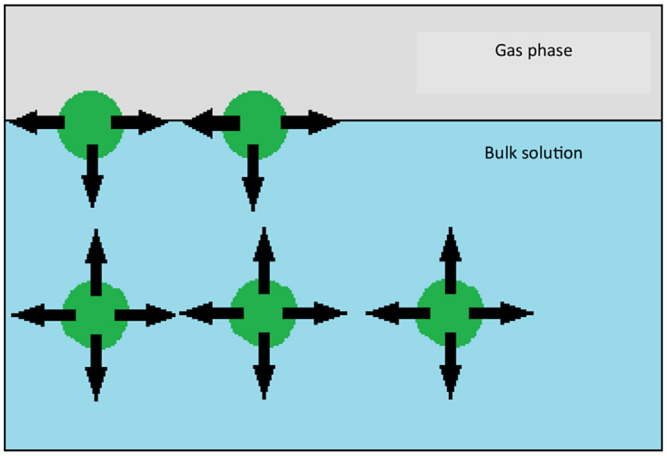

Fig. 3. Molecular attraction within the bulk solution and at the gas-liquid interface.

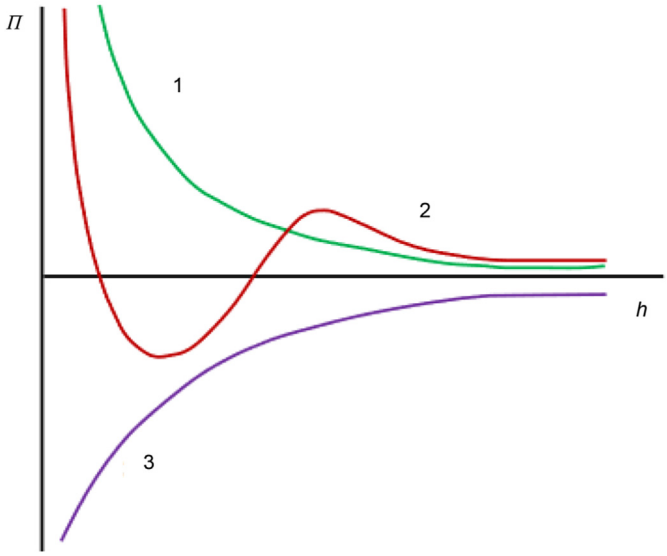

Fig. 4. Illustration from Kornev et al. (1999), in which the disjoining pressure is shown for stable films (1), metastable films (2) and unstable films (3).

subject of hydrogen bonding in all directions and are, therefore, in equilibrium. However, the hydrogen bonding of the molecules at the liquid-gas interface is not balanced, with the resulting force being directed towards the bulk phase. When a surface is created or

extended, it requires molecules to be transported from the solution to the surface; the work which is required resembles the surface tension. The surface tension is higher if the bulk liquid molecules have larger attractive forces, such as hydrogen bonding in water (Ferreira, 2019) (see Fig. 4).

The Plateau borders are connected to each other and form the network in which the liquid's gravitational drainage occurs (Soleymanzadeh et al., 2018; Akbari et al., 2019). Almost all the liquid is present in the Plateau borders for a dry foam. The two faces of a liquid film exhibit a repulsive force, which is called the disjoining pressure, working against the thinning of the film. Therefore, equilibrium in film thickness is reached when the disjoining pressure is equal to the bulk pressure of the liquid (Weaire et al., 2012; Yang et al., 2019). The difference between the gas pressure in the foam bubble and the liquid pressure in the Plateau borders is called the capillary pressure:

$$p_c = p_g - p_l \tag{1}$$

Where p_g is the pressure of gas phase and p_l pressure of liquid phase. When a positive capillary pressure is present, the disjoining pressure between the two gas-liquid interfaces prevents the films from rupturing.

The Young–Laplace equation relates the pressure difference between the gas inside a bubble and the liquid outside the bubble; the larger the bubble, the more negligible the pressure inside it. For spherical bubbles with an equal radius, the Young-Laplace equation is given:

$$p_g - p_l = \frac{2 \cdot \gamma}{r} \tag{2}$$

Where γ is the bubble radius size. However, for foam, the bubble size is usually not uniformly distributed, and therefore, the equation has to be slightly adjusted for the bubbles inside a foam (Hutzler and Weaire, 1999):

$$p_g - p_l = \frac{4 \cdot \gamma}{r} \tag{3}$$

Since the gas pressure in the bubble is uniform, the result is that the liquid pressure in the Plateau borders is lower than the pressure in the thin films. This mechanism drives the drainage from thin films towards Plateau borders. The liquid films are continuously in contact with the bulk liquid in the Plateau borders. Heat or mechanical perturbations can also influence the liquid film's thickness (Gugl, 2020).

Once the foam is generated, the stability of the foam determines how fast the foam decay takes place, which is governed by liquid drainage, coalescence and Ostwald ripening (Simjoo, 2020). Coalescence occurs when the film between two bubbles ruptures, forming one larger bubble. Mechanical shock, temperature variance, and chemicals that destroy the foam structure can also induce film rupture. Ostwald ripening is the process in which bubbles disappear due to gas diffusion from smaller to larger bubbles driven by their pressure difference (Wang et al., 2023). The diffusion mainly occurs through the thin films separating the cells, as this is the path of least resistance. As diffusion continues, the smaller bubbles will become smaller and smaller until they disappear, while the large cells grow and the foam becomes coarser (Bello et al., 2023; Bhatt et al., 2023). In the case of a homogeneous distribution of gas cells and Plateau borders, there is no variation in the pressure between cells, leading to solely gravity-driven flow. Diffusion is more difficult in wet foams as the thickness of the liquid film is larger and requires more energy to travel through. There is also a shorter distance over which diffusion can take place since the Plateau borders take up more space. Both diffusion and coalescence cause the redistribution of gas bubble sizes in the foam (Da et al., 2018; Jalilian et al., 2019).

Plateau border suction causes the liquid to be transferred from the films to the Plateau borders, from where the net buoyancy force determines the direction of gravitational drainage. The driving mechanism behind Plateau border suction is the pressure difference between the pressure in the Plateau borders and the pressure in the films (Hosseini-Nasab et al., 2019). The foam-liquid interface rises in the column as drainage takes place. As liquid drains from the films and the thickness decreases to around a few hundred nanometers, disjoining pressure ($\Pi(h)$) is described as follows:

$$\Pi(h) = \Pi_{van} + \Pi_{el} + \Pi_{ster} \tag{4}$$

Which Π_{van} is van der Waals component, Π_{el} is electrostatic and Π_{ster} is steric forces components. The main factors influencing these are surfactant type, concentration, ionic strength, and other macromolecules used to stabilize foam (Lim et al., 2023). The disjoining pressure results from an overlap of the electrical double layers as film surfaces get close to each other (Rattanaudom, 2022). The disjoining pressure slows additional drainage from the film into the Plateau borders. When the Plateau border suction is equal to the disjoining pressure in the film, mechanical equilibrium is present. Since the Plateau border suction is a function of the height position in the foam column, the equilibrium of the film thickness is as well.

This study aims to provide a comparative study of the foam stability of solutions by examining both the foam decay in time and the liquid drainage from the foam in time by offering fresh insights into the theory of foam generation, which can aid in explaining experimental results and lead to improved formulas for applied substances and concentrations. The study seeks to understand the mechanisms and structure of foam generation through laboratory experiments and theoretical analyses. The research also tries to find the importance of liquid drainage as a foam decay mechanism through interconnected Plateau borders. By comparing numerical solutions with bulk experiment outcomes, it is tried to validate the foam drainage equation and gain a more profound knowledge of foam decay mechanisms. While experimental data is limited by the lack of continuous foam conductivity measurement, foam modelling provides a more detailed understanding of different stages in foam drainage. Therefore, a comprehensive comparison and investigation of foam models are necessary to gain a deeper insight into foam behaviour.

This work advances the field of foam EOR in several ways. This study provides experimental data on foam properties, such as density and stability, under different Glycerol and polymer concentrations. It uses the Foam Scan apparatus to analyze foam behaviour over time, focusing on drainage and decay mechanisms. The study links microstructure changes to macroscopic behaviour by correlating liquid drainage with foam collapse. A mathematical model for foam drainage is presented, allowing for predictions of foam behaviour under reservoir conditions. The results indicate that higher viscosity solutions result in slower drainage rates and better liquid distribution within the foam, which could help design more stable foams for enhanced oil recovery (EOR) applications.

3. Experimental description

In order to study the properties of foams stabilized by AOS at a range of concentrations of Glycerol and polymer, the FoamScan apparatus from Teclis Instruments is used. The setup is shown in Fig. 5. A solution is injected at the side of the bottom of the glass column (D = 3.6 cm) through a connected tube, after which gas is

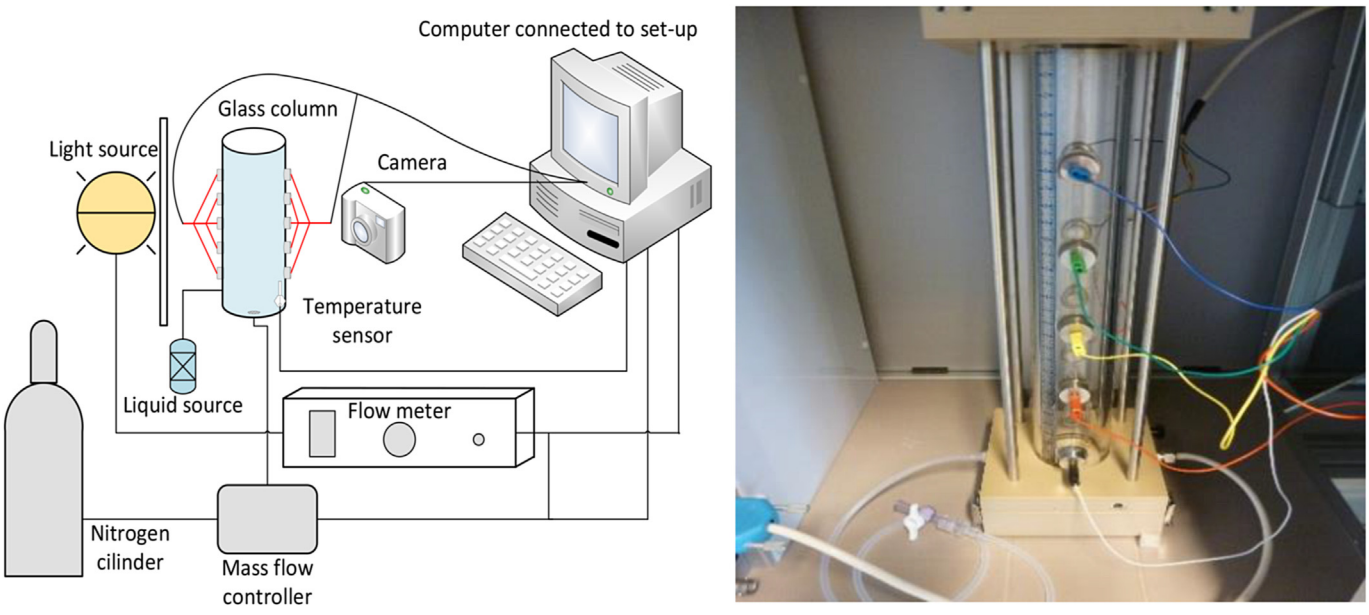

Fig. 5. The setup of the Foam Scan experiment (left), the glass column with the electrode pairs attached to it (right).

sparged from the bottom through a glass frit. Gas injection is stopped at a pre-set value for the foam height, after which the foam volume is continued to be monitored in time. The data obtained from the experiment gives insight into the behaviour of the foam in time as well as specific foam parameters such as maximum density (MD).

All experiments were conducted at room temperature and atmospheric pressure. The gas injection rate was 16 ml/min, the initial liquid volume injected was 50 cm^3, the set foam volume for which gas injection stops was 150 cm^3 and the experiment was run until at least a foam volume of 50 cm^3 or less was recorded. The nitrogen gas was used for foam generation, and a built-in mass flow meter was used for controlling the flow rate during the experiment. One wt% sodium chloride (NaCl, purchased from J.T Baker) was dissolved in deionized water for all experiments. Alpha Olefin Sulfonate $C_{14\text{-}16}$ surfactant (AOS $C_{14\text{-}16}$, Stepan, active content 39%) is used to stabilize the foam. Hydrolyzed polyacryl-amide polymer (HPAM) with a degree of hydrolysis of between 25% and 30% is used during the experiments (FLOPAAM 3530s from SNF Floerger). Glycerol Anhydrous Biochemica was purchased from Applichem Pancreac. The HPAM solution is prepared by slow vortex mixing/stirring while slowly adding the HPAM.

Research from Vikingstad et al. (2006) showed that for AOS C_{14}–C_{16} no increase in foam height was noticed when the surfactant concentration was increased from 0.5 wt% to 1.0 wt%. Therefore, in this experiment, a 0.5 wt% AOS C_{14}–C_{16} is used in all experiments. This is well above the critical micelle concentration of 0.003 wt% (Laskaris, 2015). It was shown that lower gas velocities used for foam generation lead to a smaller rate of foam drainage and a smaller extent of foam drainage. This is caused by the gas entraining less bulk solution as the foam is formed. The liquid hold profile is steeper because there is less bulk solution in the total foam column. Therefore, a fixed gas injection rate is chosen for all experiments. Even when the outcome of an experiment is that no foam is created, the gas injection rate will not be changed in order to avoid unequal experimental conditions as described (Emami et al., 2022). When gases are soluble in water (for example, CO_2), it leads to faster gas transport through the aqueous solution, which means a less stable foam than insoluble gas like nitrogen (Rio et al., 2014). This is the reason nitrogen will be used as the sparging gas.

Foam generation phase with the sparging of gas starts. After reaching the pre-set value of the foam, the gas injection and foam generation stops. CCD camera is used to capture images from foam column to analysis foam height. Foam is homogeneous when generated; therefore, the level of greyness is uniform through the foam. Foam column grey level analysis results in the actual foam height calculation. Another factor essential to measure in this experiment is the amount of liquid in the foam. The liquid level in the glass column is determined by measuring the resistance of the liquid with four electrode pairs connected to the glass tube. Before starting the experiments, the same measurement is done with the pre-injected solution to provide the conductivity of the liquid.

The quantity of liquid in the foam can be determined by analyzing the liquid level in the glass column, which can further help in establishing a correlation between the collapse of foam due to drainage and the liquid solutions applied. The FoamScan equipment can measure the foam conductivity at four levels of the glass column. The electrode pairs are measured sequentially instead of simultaneously to prevent any electrical interference and measurement errors. The relative conductivity is calculated by dividing the measured foam conductivity by the bulk liquid conductivity, and it is significantly influenced by the liquid fraction, as previously discussed by Lemlich (1978) and Weaire et al. (2012).

During the collapse phase, drainage occurs and the column's liquid height increases. A general overview of the phases in a Foam Scan experiment is shown below in Fig. 6, with Fig. 7 coinciding with points 1, 2 and 3 in Fig. 6. At point 1, time is zero, and gas sparging has not started yet. As gas sparging is initiated, point 2, foam generation starts and liquid from the pre-injected solution is distributed into the developing foam. This leads to a drop in the liquid level in the column. Point 3 is reached when the foam column has reached the pre-set foam height. At this point, the lowest liquid volume is recorded, as the liquid in the foam has reached its maximum. Gas sparging stops, after which the collapse of the foam starts. In this phase, liquid drains out of the foam, reversing the mechanism sketched in Fig. 6. The liquid eventually accumulates at the bottom of the glass column, while the foam column collapses in time from the top to the bottom.

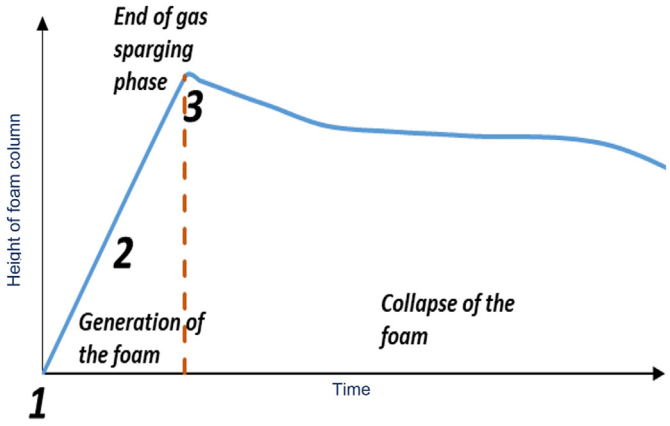

Fig. 6. Simplification of the phases during a Foam Scan experiment, with the focus on the generation of the foam.

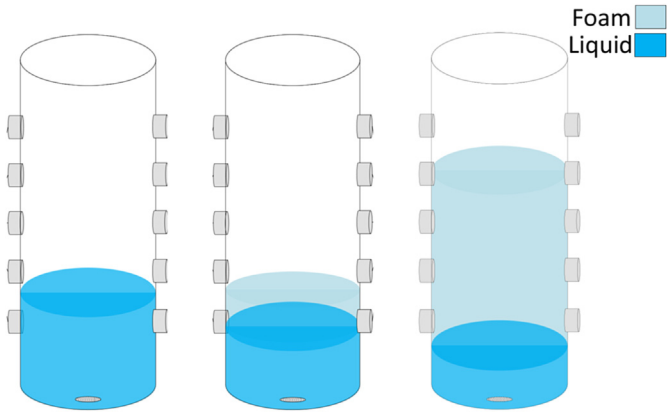

Fig. 7. Sketch of foam volume and liquid volume during the generation of foam, corresponding with Fig. 16. Left: Before gas sparging (1), Middle: During gas sparging (2), Right: End of gas sparging (3).

In order to determine the drainage of liquid, the software of the FoamScan setup calculates the liquid content based on the measured conductivity. This is built upon the findings of Lemlich (1978), who presented the relationship between the conductivity of the foam relative to that of the liquid ($\frac{\sigma_f}{\sigma_l}$) and liquid content φ_l, which is a linear approximation:

$$\frac{\sigma_f}{\sigma_l} = \frac{1}{3}\varphi_l \tag{5}$$

A spatial discretization method developed by Skeel and Berzins (1990) is used to obtain numerical solutions for the foam drainage equation. This method allows for the discretization of the equation in space, which is necessary for numerical computations. The specific software or programming language used to implement this method is MATLAB Programming language software.

The foam drainage equation is a partial differential equation that describes the mass conservation in the foam's Plateau border. It relates the cross-section area of the Plateau border (A) and the foam's average velocity (u). If u is the average velocity in the Plateau border, then conservation of mass relates the Plateau border cross-section $A(x,t)$ and u:

$$\frac{\partial A}{\partial t} + \nabla(uA) = 0 \tag{6}$$

For only one dimension, this becomes:

$$\frac{\partial A}{\partial t} + \frac{\partial}{\partial z}(uA) = 0 \tag{7}$$

The geometry of the Plateau border has been established as presented by Verbist et al. (1996) for monodispersed bubbles:

$$A = C^2 r^2 \tag{8}$$

$$C = \sqrt{\sqrt{3} - \frac{\pi}{2}} \tag{9}$$

Formula (2.8) is rewritten to write r as a function of A for future steps:

$$r = C\sqrt{A} \tag{10}$$

When one volume element $A\,dz$ is considered, a balance of the forces working on the volume element can be constructed. The three components are the gravitational force, the viscous force per unit volume and the capillary force. Laplace-Young provides the dependence of the radius of the curvature on the pressure difference between the gas in the foam bubble and the liquid present in the Plateau border:

$$p_g - p_l = \frac{\gamma}{r} \tag{11}$$

By combining (10) and (11):

$$p_l = -\frac{\gamma}{r} + p_g = -\frac{C\gamma}{\sqrt{A}} + p_g \tag{12}$$

$$\frac{\partial p_l}{\partial z} = \frac{C\gamma A^{-\frac{3}{2}}}{2}\,\frac{\partial A}{\partial z} \tag{13}$$

The gravitational forces working on the volume element are given by ρ*g.

The dissipation (the viscous forces per unit volume) is given by $-\frac{\eta u}{A}$.

The total force balance:

$$\rho g - \frac{\eta u}{A} - \frac{C\gamma A^{-\frac{3}{2}}}{2}\,\frac{\partial A}{\partial z} = 0 \tag{14}$$

Rewriting the formula to obtain the velocity function:

$$u = \frac{A\rho g}{\eta} - \frac{C\gamma A^{-\frac{1}{2}}}{2\eta}\,\frac{\partial A}{\partial z} \tag{15}$$

Finally, (13) is inserted in (5) to obtain the foam drainage equation:

$$\frac{\partial A}{\partial t} + \frac{\partial}{\partial z}\left(\frac{A^2\rho g}{\eta} - \frac{C\gamma A^{\frac{1}{2}}}{2\eta}\,\frac{\partial A}{\partial z}\right) = 0 \tag{16}$$

This foam drainage equation for one dimension was first derived by Gol'Dfarb et al. (1988). Using dimensionless variables makes it easier to solve numerically, which is why it is applied here.

Dimensionless variables: $\tau = \frac{t}{t_0}$, $\xi = \frac{z}{z_0}$, $\alpha = \frac{A}{z_0^2}$, $x_0 = \sqrt{\frac{\rho g}{C\gamma}}$ and

$t_0 = \frac{\eta}{\sqrt{\rho g C \gamma}}$ (Hutzler and Weaire, 1999).

The final dimensionless foam drainage equation is given in (15).

$$\frac{\partial \alpha}{\partial \tau} + \frac{\partial}{\partial \xi}\left(\alpha^2 - \frac{\alpha^{\frac{1}{2}}}{2}\frac{\partial \alpha}{\partial \xi}\right) = 0 \tag{17}$$

In order to solve the dimensionless foam drainage equation, two boundary conditions and one initial condition need to be specified. The initial condition is the uniformly wet foam column:

$$\alpha(\xi > 0, 0) = 1 \tag{18}$$

For the left boundary, $z = 0$, where no incoming flux is present (Hutzler and Weaire, 1999)

$$\alpha^{\frac{3}{2}}(0, \tau) - \frac{\partial}{\partial \xi}\alpha(0, \tau) = 0 \tag{19}$$

The second boundary condition is given by the liquid fraction being one at the right boundary, which is due to the presence of the liquid pool at the bottom of the foam column in the experiment.

$$\alpha(z = L) = 1 \tag{20}$$

The spatial discretization which is used is the method developed by Skeel and Berzins (1990), which is a spatial discretization method for parabolic equations in one space variable. The Matlab function ODE15s does time integration. The axis is chosen with the top of the foam being zero and increasing downwards; this is done to match the drainage direction with a positive step at the axis.

ODE15s is a function in MATLAB that is used to solve stiff differential equations. Stiff differential equations are a type of ordinary differential equations (ODEs) that involve a wide range of time scales. These equations can be challenging to solve numerically because the standard ODE solvers may require very small time steps to accurately capture the system's behaviour. ODE15s is specifically designed to handle stiff ODEs efficiently. It uses a variable-step, variable-order numerical integration method known as the backward differentiation formula (BDF) method. This method is particularly effective for stiff systems because it can automatically adjust the time step size based on the stiffness of the equations.

4. Results and discussion

4.1. Base case: 0.5 wt% AOS

To compare the foam quality and longevity of solutions containing surfactant, polymer, or Glycerol, it is necessary to conduct an experiment. The experiment involves a 0.5 wt% AOS C14–C16 and 1 wt% NaCl solution, which is repeated several times to reduce the impact of temperature and mechanical disturbance. The foam column reaches a volume of 150 cm^3, after which gas sparging is stopped, and the foam decay phase begins. The time taken for the foam volume to reach one-third of its original volume (t1/3 (V1/3 = 50 cm^3)) is used to compare the foam stability of the different experiments.

According to Fig. 8, the height of the foam column increases linearly during gas injection without any visible signs of foam destruction. The control experiment consistently shows a decay time of 3200 ± 200 s for a volume of 75 cm^3 and 4100 ± 200 s for a volume of 50 cm^3. These times are measured from the moment gas sparging stops. The liquid volume in the foam increases rapidly during the foaming phase, followed by a decrease at almost the same rate as it increased during injection until a liquid volume of approximately 5 cm^3 is reached. After this point, the drainage rate slows until no liquid is detected in the foam after 1500 s day time. Film thinning due to drainage is the primary factor leading to film rupture and further foam decay.

After a period of minimal foam decay, known as the plateau phase, a second, more extensive decay phase of the foam volume occurs. This decay is not caused by drainage, as all liquid has already drained out of the foam, but rather by either bubble coalescence or Oswald Ripening. The experiment is halted once the foam volume reaches a final volume of 50 cm^3 or less.

It is crucial to differentiate between these foam decay mechanisms to understand the potential differences in decay trends for various solutions. The initial decrease in foam volume from t = 500 s to t = 900 s in Fig. 8 is primarily due to liquid draining out of the foam under the influence of gravity, which is evident from the significant drop in liquid volume in the foam during the same time frame. This can be confirmed by plotting both data sets together, as seen in Fig. 9 for the mentioned period. The foam volume decay during this period is (150.8−136.9) = 13.9 cm^3, while the liquid volume decay in the foam is (17.3−5.0) = 12.3 cm^3. Liquid drainage is the dominant mechanism for foam decay in the early stages after gas sparging has ceased.

The result of the numerical simulation is shown in Figs. 10 and 11. Initially, the drainage of the liquid at the top of the column occurs fast, while no change occurs at the bottom of the foam column where the foam stays wet. After some time, the profile of the liquid content in the foam is a linear profile, from where it starts to converge to the steady-state solution as the front propagates through the column and reaches the bottom.

Fig. 11 shows the total numerical solution of the foam drainage equation for the Plateau border area for each time and depth. It shows the transformation of the Plateau border area profile in more detail; the rapid liquid drainage out of the very top of the foam column followed by a more linear profile, resulting in an equilibrium state with a finite Plateau border area.

The choice of dimensionless parameters shows that when a change is made in the viscosity of the fluid, for example, $\eta_2 = 2{*}\eta$, the solution would only be affected for the dimensionless time. Hence, for $\eta_2 = 2{*}\eta$, the solution of the foam drainage equation will reach the equilibrium state after a dimensionless time that is twice as large as for $\eta_1 = \eta$. The profile of the distribution of the liquid content throughout the vertical column is not altered by a change in viscosity.

An implementation of the viscosity of the fluid subjected to drainage into the foam drainage equation leads to Fig. 12, Figs. 13 and 14. These figures show the numerical solution at dimensionless times 5, 10 and 50 for $\eta_1 = 1{*}\eta$, $\eta_2 = 2{*}\eta$ and $\eta_3 = 3{*}\eta$ <! – – Q4 : **Fig**. **15** was not cited in the text. Please check that the citation (s) suggested are in the appropriate place, and correct if necessary. – – > (see Fig. 15).

As the foam drainage at t = 10 in Fig. 13 reaches the linear state for the least viscous solution, the double and triple viscous solutions still exhibit asymptotic behaviour.

Fig. 14 shows the solutions converging towards the steady state solution, which is reached earlier for the less viscous solutions.

The numerical solutions show the foam drainage rate's dependency on the bulk liquid's viscosity. This aspect will be investigated thoroughly in the following. To gain a more profound knowledge and analyze the viscosity effect on foam stability, it was tried to compare the effect of different concentrations of polymer and Glycerol. In the following, this comparison can be observed.

As the figures exhibit, the higher the concentration, the higher the liquid content in the foam (see Fig. 16). It means that the high concentrations of Glycerol and HPAM polymer are able to hold up liquid content in foam lamella longer compared to lower concentrations. This result is in accordance with the experimental results of foam stability with different concentrations of Glycerol and

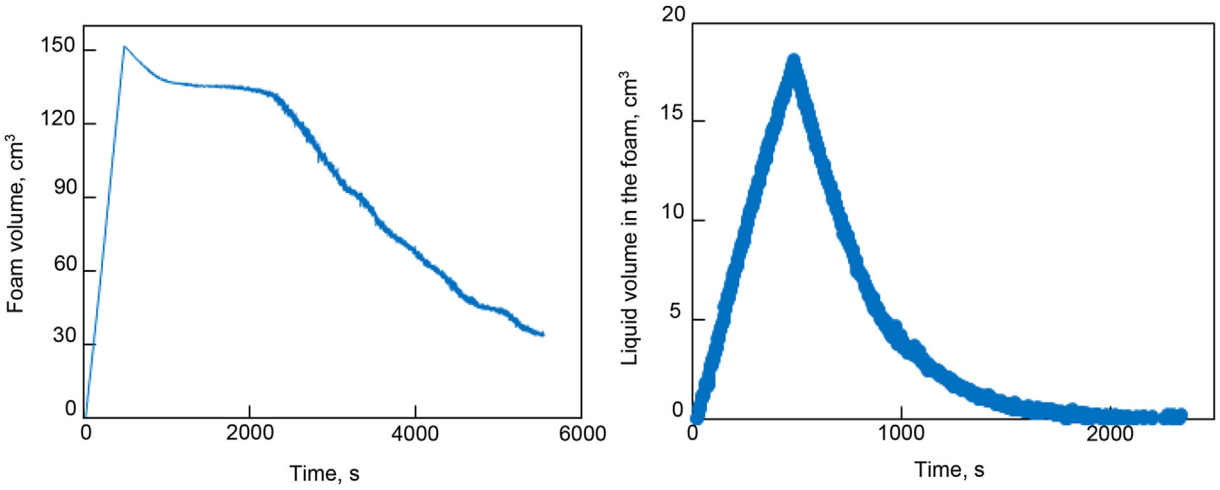

Fig. 8. Foam volume versus time for the control experiment (left) and the liquid volume in the foam versus time for the control experiment (right).

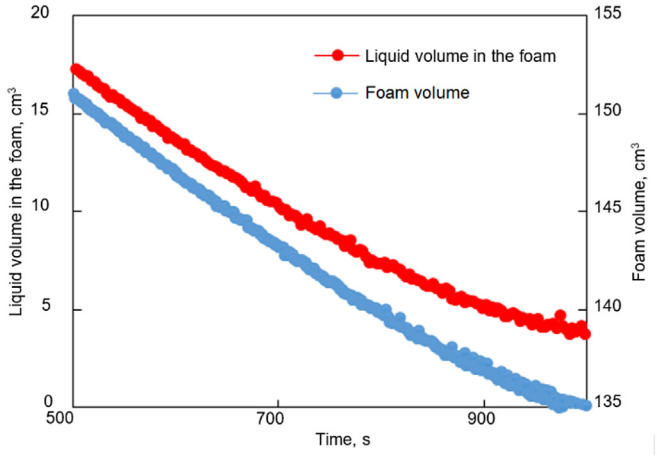

Fig. 9. Observation of liquid drainage as the main cause for initial foam height decay showing that they are completely in direct convergence.

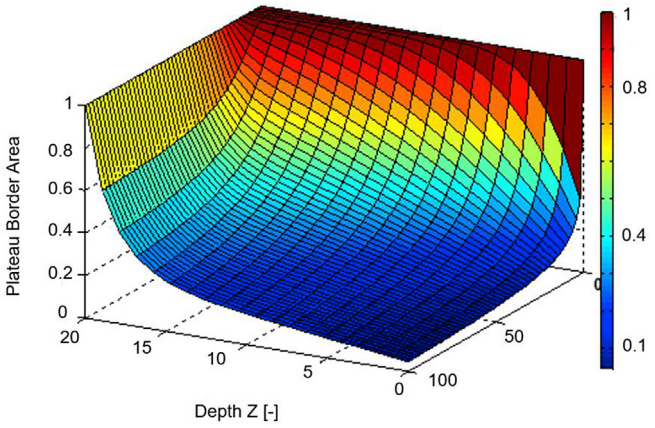

Fig. 11. Complete numerical solution of the Plateau border area in time and depth, obtained from solving the foam drainage equation.

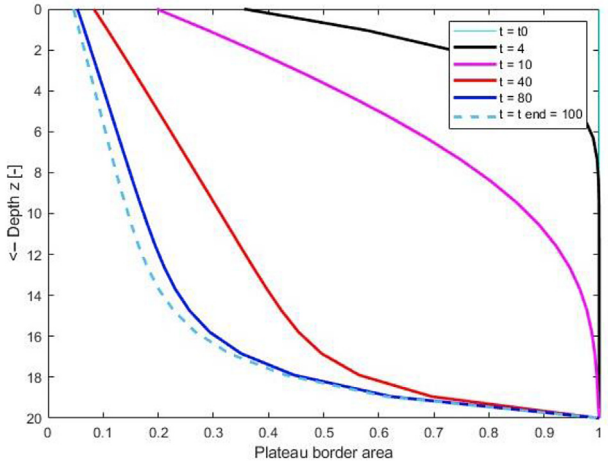

Fig. 10. Numerical solution of the foam drainage equation. It indicates the liquid drainage is significantly faster at the top of the foam column.

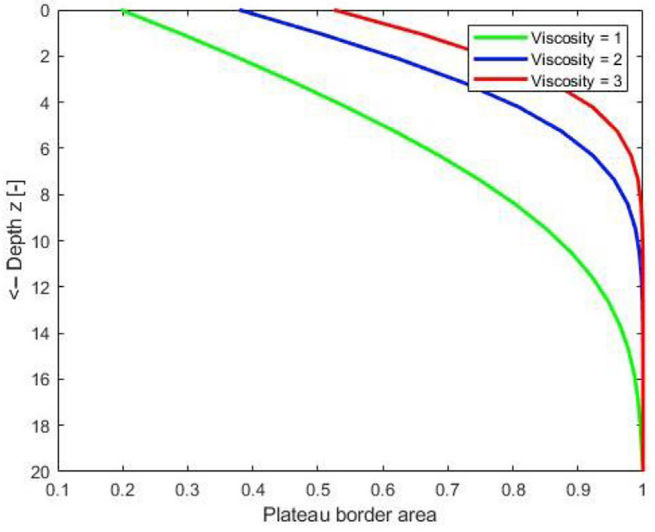

Fig. 12. Numerical solution of foam drainage equation for different viscosities, at t = 5. It indicates the higher the viscosity, the higher foam can contain liquid contents in lamella.

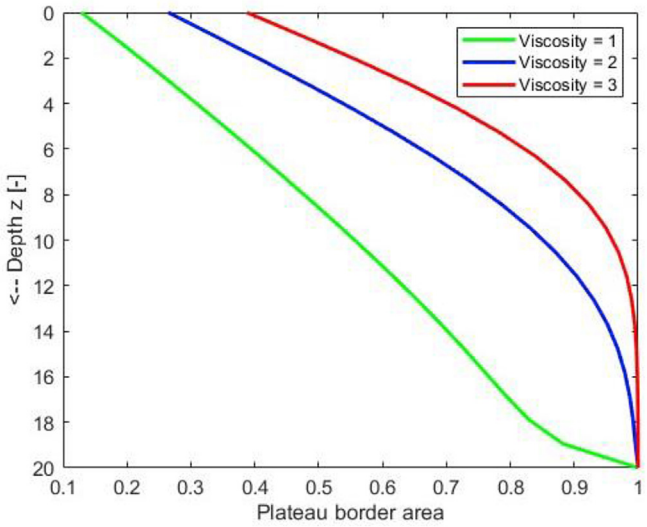

Fig. 13. Numerical solution of foam drainage equation for different viscosities, at t = 10. Less viscous foam shows faster drainage and reaches the steady-state solution faster.

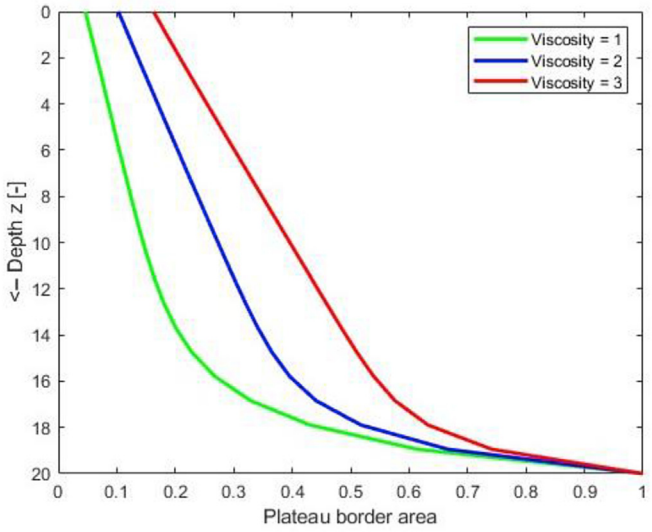

Fig. 14. Numerical solution of foam drainage equation for different viscosities, at t = 50. Foam with higher viscosity contains higher liquid content at the upper parts of the column and slower drainage.

HPAM. The results are provided in Figs. 17 and 18.

These figures represent the decrease in drainage and higher foam stability by increasing the viscosity of the bulk liquid. The liquid volume in the foam during the experiment gives insight into the ability of the bulk liquid solution to be brought into the foam and the ability of the foam to retain the liquid once it is there. Foam destruction is an effect of film thinning. Film thinning is due to liquid drainage until almost all liquid is gone and other destruction mechanisms take over. Therefore, the liquid volume in the foam provides information about which destruction mechanism is dominant.

4.2. Comparison of the numerical solution with the bulk foam experiment

The previously described numerical solution of the foam drainage equation gives the distribution of the liquid fraction over the height of the foam column but then in dimensionless parameters. In order to compare the solution with a bulk foam experiment, it would be beneficial to have a continuous measurement of

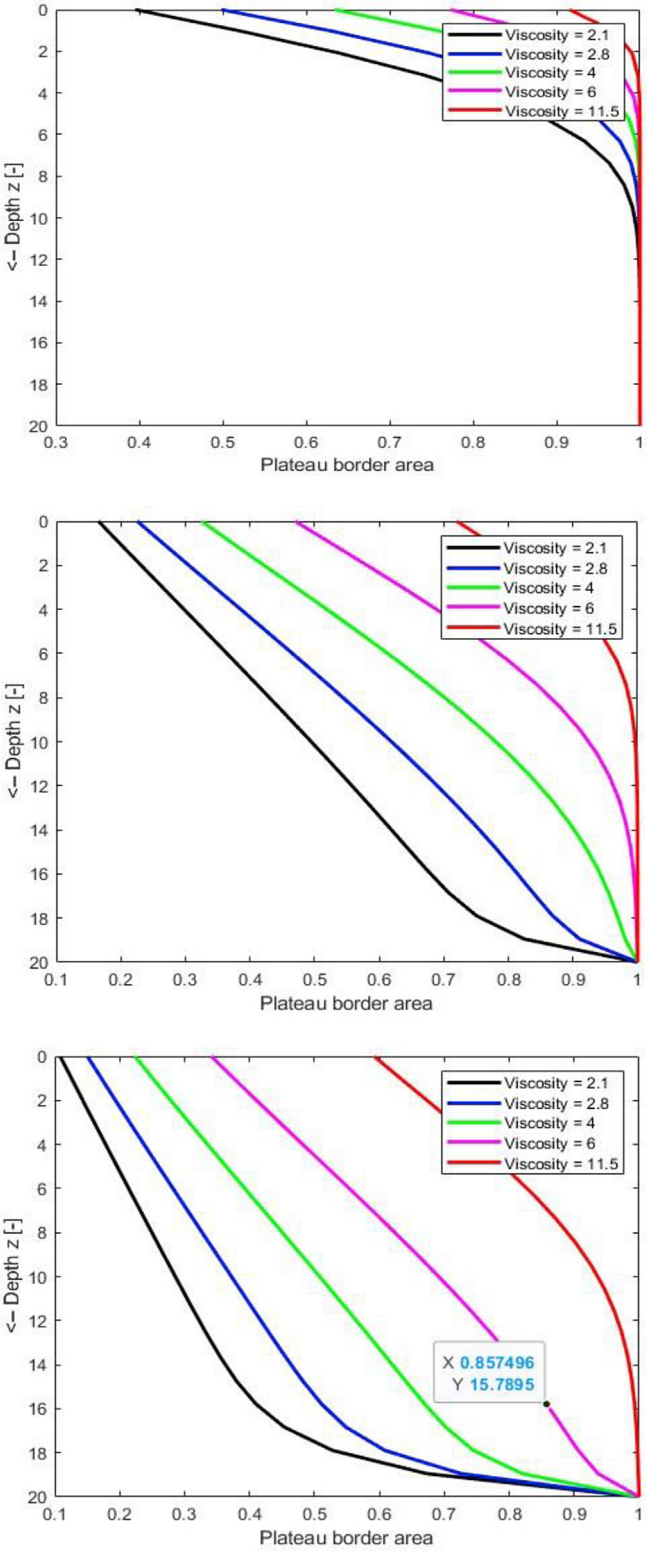

Fig. 15. Numerical solution of foam drainage equation for different viscosities of Glycerol. a: T = 5 s, b: T = 25 s, c: T = 50 s. It can be observed that higher concentrations lead to foam with higher liquid content and lower foam drainage.

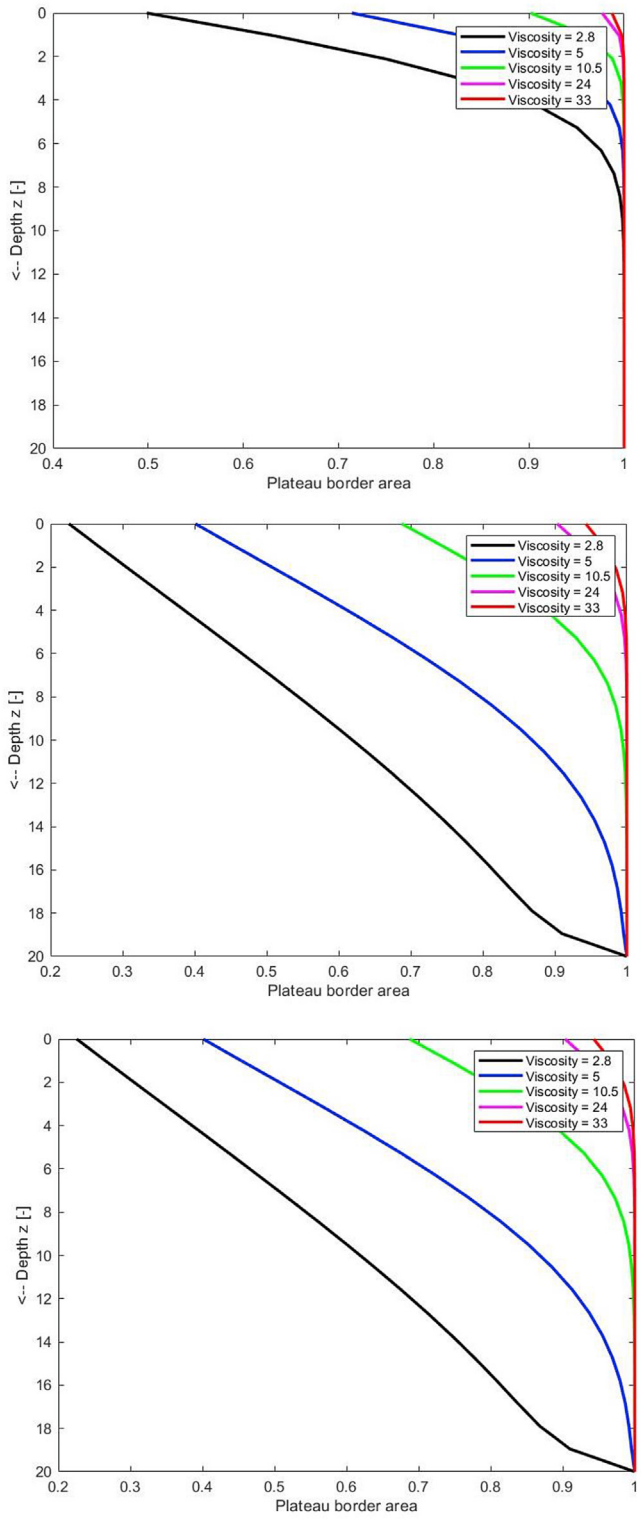

Fig. 16. Numerical solution of foam drainage equation for different viscosities of HPAM polymer. a: T = 5 s, b: T = 25 s, c: T = 50 s. It shows that higher concentrations of HPAM polymer can hold liquid content more than lower concentrations, which leads to foam stability improvements. According to it, for the least viscous solution reaches linear stage solution faster, viscous solutions still exhibit asymptotic behaviour. Compared with glycerol foam liquid content simultaneously, HPAM polymer, due to higher viscosities than Glycerol, results in higher liquid content and higher foam stability.

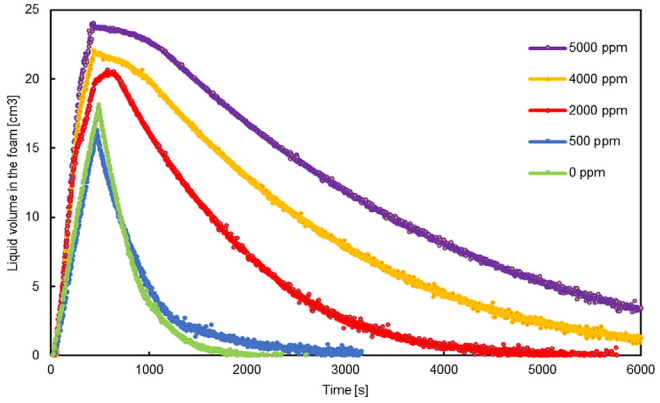

Fig. 17. Retained liquid volume in foam for different concentrations of HPAM. As observed and concluded in numerical solution of foam drainage equation, experimental results show that a higher concentration of HPAM polymer results in higher foam stability and drainage.

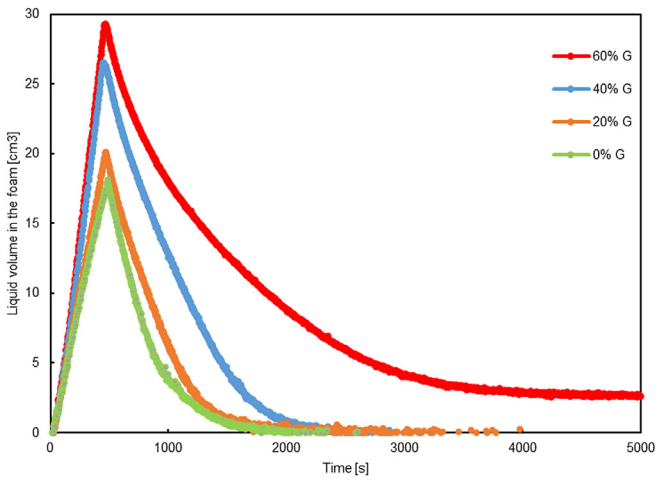

Fig. 18. Retained liquid volume in foam for different concentrations of Glycerol. Glycerol foam with higher viscosity shows a lower drainage rate and higher liquid content than others. However, it still shows a faster drainage rate than HPAM polymer foam.

the conductivity over the height of the foam column to establish the liquid fraction over the whole foam column. Unfortunately, the Foam Scan apparatus does not provide continuous measurement over the height, but it has four pairs of electrodes at several intervals over the height of the column instead. The previous bulk foam experiments were conducted with a pre-set maximum foam height, after which gas sparging was stopped. During these experiments, not all four electrode pairs were reached by the foam, while the information of four electrode pairs is beneficial for the comparison with the numerical solution. Therefore, the same setup is used, with the difference that the pre-set value of the foam height is set at the maximum height. The gas injection rate is set at 30 ml/min to ensure the desired foam height will be reached. After the experiment is finished, the data from the four electrode pairs is used to create Fig. 19. The numerical solution is shown in Fig. 20. It shows that it indeed is a satisfactory approximation of the liquid drainage in the foam, the general trend of the liquid fraction converging to a linear profile from its original value at t_0, after which the equilibrium profile is reached. However, both results have a large difference concerning the liquid fraction profile at t = 0. First, the numerical solution starts with the initial condition

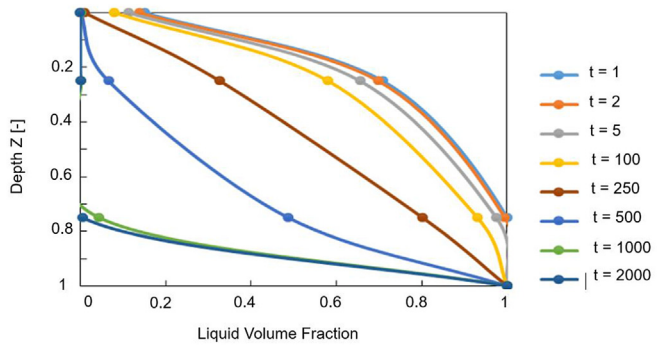

Fig. 19. Liquid volume fraction as measured in FoamScan experiment. By comparing the numerical solution result of foam drainage, satisfactory resemblance and similar trend is observable.

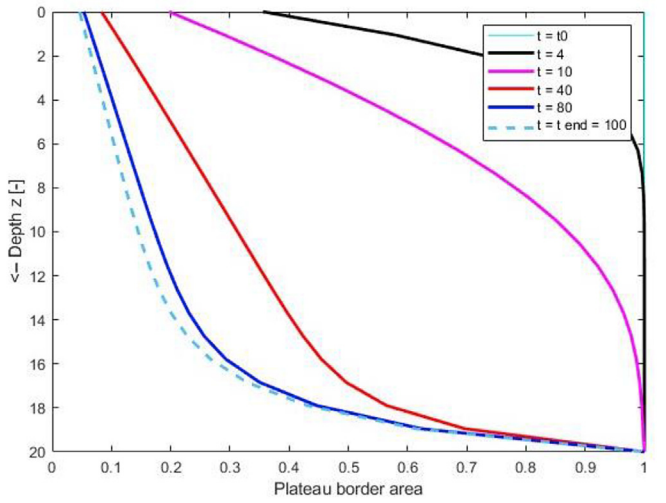

Fig. 20. The numerical solution of the foam drainage equation. Due to the appointed boundary condition, at t = t0, a high liquid fraction can be observed, which contrasts with real experiment result.

of a fully wet foam column, while in reality, this cannot be achieved by the generation of foam with the method described above. The liquid at the top of the foam will already drain out during the formation of the foam.

The second significant difference occurs at the lower limit of the liquid fraction. The numerical solution has a finite limit due to the boundary condition which is in place. For the result from the bulk experiment, however, there is no information on the lower limit of the liquid fraction due to the lack of continuous electrodes along the column height. Therefore, the liquid-gas interface gives the lower limit, where the liquid fraction is of a value of 1.

Third, the foam drainage equation is constructed upon certain assumptions which are not 100% in accordance with the actual physics, mainly the assumption that the foam is entirely homogenous (this assumption describes the Plateau border area). The possibility of evaporation occurring is also not considered, which, although it could be a small factor, is present in experimental conditions. Despite these discrepancies, the foam drainage equation proves to be a satisfactory model of drainage in standing foam.

5. Conclusions

In conclusion, the experiment aimed to compare the foam quality and longevity of solutions containing surfactant, polymer, or Glycerol. The foam stability was evaluated by measuring the time taken for the foam volume to reach one-third of its original volume (t1/3). The results showed that the initial decrease in foam volume was primarily due to liquid drainage under the influence of gravity. Film thinning due to drainage was identified as the primary factor leading to foam decay.

Numerical solutions of the foam drainage equation were obtained to further analyze the foam behaviour. The results indicated that higher concentrations of Glycerol and HPAM polymer led to higher liquid content in the foam and lower foam drainage rates, resulting in improved foam stability. The numerical solution provided a satisfactory approximation of the liquid drainage in the foam, although there were discrepancies with the actual experimental results, particularly at the initial and lower limits of the liquid fraction.

It is important to note that the foam drainage equation assumes certain ideal conditions, such as a completely homogeneous foam and the absence of evaporation. These assumptions may not fully align with the actual experimental conditions. Despite these discrepancies, the foam drainage equation proved helpful in understanding foam behaviour and predicting foam stability.

Further experiments with continuous measurement of conductivity over the height of the foam column would provide more accurate data for comparison with the numerical solution. Overall, the study contributes to our understanding of foam stability and provides insights into the effects of different solutions on foam quality and longevity.

The numerical solution of the foam drainage equation starts with a high liquid fraction at t = t0 due to the specified boundary condition. However, in real experiments, the liquid at the top of the foam drains out during the formation of the foam, resulting in a lower initial liquid fraction. This is a discrepancy between the numerical solution and the actual experimental results. However, further investigation is necessary to fully understand the physical dynamics of foam stability and decay and to validate the model assumptions, such as exploring the influence of external parameters such as temperature, pressure or other foam properties such as foam density bubble size distribution.

Parameters list

$Q =$ volumetric flow rate $\left(\frac{m^3}{s}\right)$

$D =$ Foam Column Diameter (m)

$r =$ Foam column radius (m)

$A =$ *Foam column Area* $\left(m^2\right)$

$u =$ Flow velocity $\left(\frac{m}{s}\right)$

$k =$ pearmeability $(Darcy)$

$\varphi =$ Prosity

$\dot{y}_{\mathrm{pm}} = \alpha' * \frac{4u}{\sqrt{8 * k * \varphi}} =$ Shear Rete $(\alpha' = constant)$

CRediT authorship contribution statement

S.M. Hosseini-Nasab: Writing – review & editing, Validation, Supervision, Project administration. **M. Rezaee:** Writing – original draft, Validation. **P.L.J. Zitha:** Supervision.

Declaration of competing interest

There is no conflict of interest about the manuscript.

Acknowledgment

We express our gratitude to Shell Global Solution BV for their provision of chemicals and assistance in conducting certain experiments at the Rock & Fluid Physics Laboratory of Shell Global Solution Company in Rijswijk, The Netherlands. We extend our appreciation to E Meivogel and J van Haagen for their technical support at the Dietz Laboratory of the Geoscience and Engineering Department of Delft University of Technology. This manuscript was collaboratively prepared by all authors, who contributed to its conception, design, and execution, and have reviewed and approved the final version.

References

Abdelaal, A., Gajbhiye, R., Al-Shehri, D., 2020. Mixed CO_2/N_2 foam for EOR as a novel solution for supercritical CO_2 foam challenges in sandstone reservoirs. ACS Omega 5 (51), 33140–33150.

Ahmed, S., Elraies, K.A., Hanamertani, A.S., Hashmet, M.R., Shafian, S.R., Hsia, I.C., 2019. Investigation of carbon dioxide foam performance utilizing different additives for fracturing unconventional shales. In: SPE Abu Dhabi International Petroleum Exhibition and Conference.

Akbari, S., Mahmood, S.M., Nasr, N.H., Al-Hajri, S., Sabet, M., 2019. A critical review of concept and methods related to accessible pore volume during polymer-enhanced oil recovery. J. Petrol. Sci. Eng. 182, 106263.

Ardakani, A.G., Mohammadi Alamooti, A.H., Rasaei, M.R., Javadi, A., Ghazanfari, M.H., Davarzani, H., 2020. Monitoring polymer-enhanced foam displacements through heterogeneous porous media: a pore-scale study. J. Energy Resour. Technol. 142 (7), 073003.

Bai, B., Leng, J., Wei, M., 2022. A comprehensive review of in-situ polymer gel simulation for conformance control. Petrol. Sci. 19 (1), 189–202.

Bello, A., Ivanova, A., Cheremisin, A., 2023. Foam EOR as an optimization technique for gas EOR: a comprehensive review of laboratory and field implementations. Energies 16 (2), 972.

Bhatt, S., Saraf, S., Bera, A., 2023. Perspectives of foam generation techniques and future directions of nanoparticle-stabilized CO_2 foam for enhanced oil recovery. Energy Fuel. 37 (3), 1472–1494.

Bouquet, S., Douarche, F., Roggero, F., Bourbiaux, B., 2019. Numerical assessment and optimization of foam-based EOR processes in naturally fractured carbonate oil-wet reservoirs. In: IOR 2019–20th European Symposium on Improved Oil Recovery. European Association of Geoscientists & Engineers.

Burrows, L.C., Haeri, F., Cvetic, P., Sanguinito, S., Shi, F., Tapriyal, D., Goodman, A., Enick, R.M., 2020. A literature review of CO_2, natural gas, and water-based fluids for enhanced oil recovery in unconventional reservoirs. Energy Fuel. 34 (5), 5331–5380.

Da, C., Alzobaidi, S., Jian, G., Zhang, L., Biswal, S.L., Hirasaki, G.J., Johnston, K.P., 2018. Carbon dioxide/water foams stabilized with a zwitterionic surfactant at temperatures up to 150° C in high salinity brine. J. Petrol. Sci. Eng. 166, 880–890.

Davarpanah, A., Mirshekari, B., 2020. Numerical simulation and laboratory evaluation of alkali–surfactant–polymer and foam flooding. Int. J. Environ. Sci. Technol. 17 (2), 1123–1136.

Dong, X., Liu, H., Hou, J., Liu, G., Chen, Z., 2016. Polymer-enhanced foam PEF injection technique to enhance the oil recovery for the post polymer-flooding reservoir. In: SPE Western Regional Meeting.

Emami, H., Ayatizadeh Tanha, A., Khaksar Manshad, A., Mohammadi, A.H., 2022. Experimental investigation of foam flooding using anionic and nonionic surfactants: a screening scenario to assess the effects of salinity and ph on foam stability and foam height. ACS Omega 7 (17), 14832–14847.

Ferreira, V.H., 2019. Injection scheme to reduce retention and improve economics of polymer enhanced oil recovery. In: SPE Annual Technical Conference and Exhibition.

Gol'Dfarb, I.I., Kann, K.B., Shreiber, I.R., 1988. Liquid flow in foams. Fluid Dynam. 23 (2), 244–249.

Goodarzi, F., Zendehboudi, S., 2019. Effects of salt and surfactant on interfacial characteristics of water/oil systems: molecular dynamic simulations and dissipative particle dynamics. Ind. Eng. Chem. Res. 58 (20), 8817–8834.

Gugl, R., 2020. Modelling and Simulation of Foam-Assisted Water-Alternating-Gas Injection in Naturally Fractured Carbonate Reservoirs (Doctoral Dissertation). University of Leoben.

Hanamertani, A.S., Ahmed, S., 2021. Probing the role of associative polymer on $scCO_2$-Foam strength and rheology enhancement in bulk and porous media for improving oil displacement efficiency. Energy 228 (2), 120531.

Hernando, L., Bertin, H.J., Omari, A., Dupuis, G., Zaitoun, A., 2016. Polymer-enhanced foams for water profile control. In: SPE Improved Oil Recovery Conference.

Hosseini-Nasab, S.M., Zitha, P.L., Mirhaj, S.A., Simjoo, M., 2015. A new chemical enhanced oil recovery method?. In: SPE International Conference on Oilfield Chemistry?.

Hosseini-Nasab, S.M., Padalkar, C., Battistutta, E., Zitha, P.L.J., 2016. Mechanistic modeling of the alkaline/surfactant/polymer flooding process under sub-optimum salinity conditions for enhanced oil recovery. Ind. Eng. Chem. Res. 55 (24), 6875–6888.

Hosseini-Nasab, S.M., Zitha, P.L.J., 2017. Investigation of chemical-foam design as a novel approach toward immiscible foam flooding for enhanced oil recovery. Energy Fuel. 31 (10), 10525–10534.

Hosseini-Nasab, S.M., Simjoo, M., 2018. Experimetal study and numerical modelling of the effect of foaming agent properties on foam flooding in porous media in absence of oleic phase. In: SPE Europec Featured at EAGE Conference and Exhibition?.

Hosseini-Nasab, S.M., Taal, M., Zitha, P.L., Sharifi, M., 2019. Effect of Newtonian and non-Newtonian viscosifying agents on stability of foams in enhanced oil recovery. Part I: under bulk condition. Iran. Polym. J. (Engl. Ed.) 28, 291–299.

Hosseini-Nasab, S.M., Rezaee, M., Taal, M., Zitha, P.L., 2022. Investigation of foam flooding assisted by non-Newtonian and novel Newtonian viscosifying agents for enhanced oil recovery. ACS Omega 8 (1), 297–310.

Hutzler, S., Weaire, D.L., 1999. The Physics of Foams. Oxford University Press, Oxford.

Imuetinyan, H., Agi, A., Gbadamosi, A., Junin, R., Oseh, J., 2022. Oil-water interfacial tension, wettability alteration and foaming studies of natural surfactant extracted from Vernonia Amygdalina. Petrol. Res. 7 (3), 350–356.

Issakhov, M., Shakeel, M., Pourafshary, P., Aidarova, S., Sharipova, A., 2022. Hybrid surfactant-nanoparticles assisted CO_2 foam flooding for improved foam stability: a review of principles and applications. Petrol. Res. 7 (2), 186–203.

Jalilian, M., Tabzar, A., Ghasemi, V., Mohammadzadeh, O., Pourafshary, P., Rezaei, N., Zendehboudi, S., 2019. An experimental investigation of nanoemulsion enhanced oil recovery: use of unconsolidated porous systems. Fuel 251, 754–762.

Kornev, K.G., Neimark, A.V., Rozhkov, A.N., 1999. Foam in porous media: thermodynamic and hydrodynamic peculiarities. Adv. Colloid Interface Sci. 82 (1–3), 127–187.

Laskaris, G., 2015. Effect of Surfactant Concentration, Water Treatment Chemicals, Fatty Acids and Alcohols on Foam Behavior in Porous Media and in Bulk (Master Thesis). Delft University of Technology.

Lemlich, R., 1978. A theory for the limiting conductivity of polyhedral foam at low density. J. Colloid Interface Sci. 64 (1), 107–110.

Lim, S.S.S., Elochukwu, H., Nandong, J., Bennour, Z., Hamid, M.A., 2023. A review on the mechanisms of low salinity water/surfactant/nanoparticles and the potential synergistic application for c-EOR. Petrol. Res. 8 (3), 324–337.

Rattanaudom, P., Shiau, B.J.B., Harwell, J.H., Suriyapraphadilok, U., Charoensaeng, A., 2022. The study of ultralow interfacial tension SiO2-surfactant foam for enhanced oil recovery. J. Petrol. Sci. Eng. 209, 109898.

Razavi, S.M.H., Shahmardan, M.M., Nazari, M., Norouzi, M., 2020. Experimental study of the effects of surfactant material and hydrocarbon agent on foam stability with the approach of enhanced oil recovery. Colloids Surf. A Physicochem. Eng. Asp. 585, 124047.

Rezaee, M., Hosseini-Nasab, S.M., Fahimpour, J., Sharifi, M., 2022. New Insight on improving foam stability and foam flooding using fly-ash in the presence of crude oil. J. Petrol. Sci. Eng. 214, 110534.

Rio, E., Drenckhan, W., Salonen, A., Langevin, D., 2014. Unusually stable liquid foams. Adv. Colloid Interface Sci. 205, 74–86.

Roozbahani, A., Soofivand, F., Al-Tameemi, A.S.H., Abdollahi, H., Saatchi, S., Ansari, A., 2024. A contrasting analysis of CO_2 and N_2 foam flood for enhanced oil recovery and geological storage of CO_2. Petrol. Res.9 1, 55–60.

Simjoo, M., Zitha, P.L.J., 2020. Modeling and experimental validation of rheological transition during foam flow in porous media. Transport Porous Media 131, 315–332.

Skauge, A., Solbakken, J., Ormehaug, P.A., Aarra, M.G., 2020. Foam generation, propagation and stability in porous medium. Transport Porous Media 131 (1), 5–21.

Skeel, R.D., Berzins, M., 1990. A method for the spatial discretization of parabolic equations in one space variable. SIAM J. Sci. Stat. Comput. 11 (1), 1–32.

Soleymanzadeh, A., Gahrooei, H.R.E., Joekar-Niasar, V., 2018. A new empirical model for bulk foam rheology. J. Energy Resour. Technol. 140 (3).

Verbist, G., Weaire, D., Kraynik, A.M., 1996. The foam drainage equation. J. Phys. Condens. Matter 8 (21), 3715.

Vikingstad, A.K., Aarra, M.G., Skauge, A., 2006. Effect of surfactant structure on foam–oil interactions: comparing fluorinated surfactant and alpha olefin sulfonate in static foam tests. Colloids Surf. A Physicochem. Eng. Asp. 279 (1–3), 105–112.

Wang, J., Yang, W., Geng, J., Shao, Z., Song, W., 2023. Experimental investigation on degradation mechanism of membrane electrode assembly at different humidity under automotive protocol. Chin. J. Chem. Eng. 56, 70–79.

Wang, Z., Liu, X., Luo, H., Peng, B., Sun, X., Liu, Y., Rui, Z., 2021. Foaming properties and foam structure of produced liquid in alkali/surfactant/polymer flooding

production. J. Energy Resour. Technol. 143 (10).
Weaire, D., Tobin, S.T., Meagher, A.J., Hutzler, S., 2012. Foam morphology. Foam Engineering: Fundamentals and Applications, pp. 5–26.
Xu, X., Saeedi, A., Liu, K., 2017. Experimental study on a novel foaming formula for CO_2 foam flooding. J. Energy Resour. Technol. 139 (2).
Yang, J., Wang, X., Yang, Y., Peng, X., Zeng, F., 2019. An empirical model to estimate sweep efficiency of a surfactant-alternating-gas foam process in heterogeneous reservoirs. J. Energy Resour. Technol. 141 (12).
Yu, Y., Saraji, S., 2021. Supercritical CO_2 foam stabilized by a viscoelastic surfactant in fractured porous media: the effect of fracture surface roughness. Energy Fuel. 35 (12), 10051–10061.
Yusuf, S.M., Junin, R., Sidek, M.A.M., Manan, M.A., Fuad, M.F.I.A., Jaafar, M.Z., Yahya, E., Rosli, N.R., 2022. The effect of nanosilica sizes in the presence of nonionic TX100 surfactant on CO_2 foam flooding. Petrol. Res. 7 (1), 62–76.
Zhang, Y., Chang, Z., Luo, W., Gu, S., Li, W., An, J., 2015. Effect of starch particles on foam stability and dilational viscoelasticity of aqueous-foam. Chin. J. Chem. Eng. 23 (1), 276–280.
Zhao, F., Wang, K., Li, G., Zhu, G., Liu, L., Jiang, Y., 2022. A review of high-temperature foam for improving steam flooding effect: mechanism and application of foam. Energy Technol. 10 (3), 2100988.
Zoeir, A., Simjoo, M., Chahardowli, M., Hosseini-Nasab, M., 2020. Foam EOR performance in homogeneous porous media: simulation versus experiments. J. Pet. Explor. Prod. Technol. 10 (5), 2045–2054.